JAST, 2018;11(1):29-43

COANDA SURFACE EFFECT ON THE SWEEPING JET ACTUATOR

Bartosz JUREWICZ SLUPSKI

Khalifa University of Science and Technology,
Abu Dhabi, 127788, UAE,
bartosz.slupski@kustar.ac.ae

Kursat KARA*

Khalifa University of Science and Technology
Abu Dhabi, 127788, UAE,
kursat.kara@kustar.ac.ae

Accepted: *19th December 2017*

ABSTRACT

A sweeping jet (SWJ) actuator emits a continuous but spatially oscillating jet when pressurized with a fluid. In this study, unsteady flow fields generated by an SWJ actuator are investigated using two-dimensional, unsteady, Reynolds-Averaged Navier Stokes (2D-URANS) simulations with Ansys v17 Fluent software over a nine different Coanda Surfaces. As a turbulence model, the SST k-ω has been used in the numerical simulations. At a characteristic point, oscillating jet velocity magnitude is sampled, and a Fast Fourier Transform (FFT) performed for several SWJ models. The jet oscillation frequency of the baseline case was compared with experimental and other numerical studies in the literature, and an excellent agreement was found. Using the validated simulation model, several modified Coanda Surfaces were studied. The effect of different Coanda surface, as well as mass flow rate on the jet velocity profile, is presented. Additionally, the static and total pressure is analyzed to determine the pressure drop of each modified SWJ actuator.

Keywords*: Sweeping Jet Actuator, Coanda Surface, Active Flow Control, CFD.*

1. INTRODUCTION

Air passenger traffic increased exponentially [1] over last decades. This forced the civil aeronautical industry to focus the new aircraft design [2] improving the sustainability, operational effectiveness and the reduction of the fuel cost. The active flow control [3] (AFC) is an innovative technology enclosed to this objective with the main objective of reducing the necessary burn fuel and decrease the operational cost. The active fuel control can be performed by actuators [4]. Actuators are devices that convert an electrical signal into a desired physical quantity. The type of actuator that will be studied in this paper is a fluidic oscillator called Sweeping Jet (SWJ) Actuator [4-6]. The SWJ actuator generates an oscillating jet when is supplied with a mass flow in the inlet. The basic design of the SWJ does not include any moving parts. During many years, the SWJ actuators have been used in irrigation systems [7] and windshield washer systems with water as the primary fluid. The detailed flow physics has still to be understood [8, 9]. The effect of some geometric parameters of the feedback channels have been recently studied [9], but further geometric details need investigation. The advantages of SWJ actuator are a large disturbance; easy to manufacture as doesn't involve moving parts; a long range of sizes and hence large frequencies. Additionally, this actuator can be turned on only during the necessary time [10]. However, the main disadvantage is that an SWJ actuator requires an external mass flow supply to operate. The primary application of the SWJ actuators is found in the flow control on the vertical tail [11-14]. The vertical tail is a huge surface that is designed with oversized parameters to perform emergency take off with the one engine out a scenario or crosswind landing/take-off. During the cruise, the dynamic pressure around the vertical tail has a substantial value, and small rudder deflections are adequate to generate yaw moment. The opposite occurs in the take off when the flow moving around the vertical tail is slower, then larger deflections are required. Moreover, this is the reason for the oversized vertical tails. However, the SWJ actuator can be the solution to manufacture a smaller vertical tail with the same or superior performance

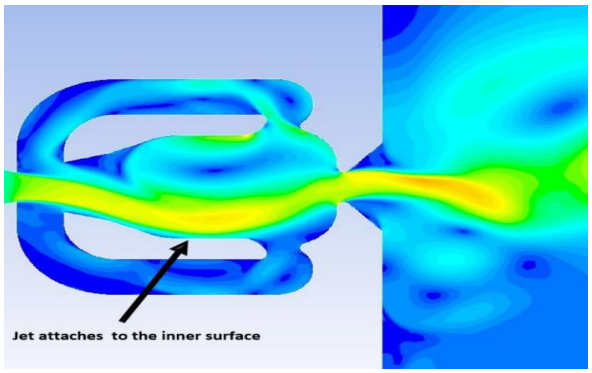

Figure 1. Sweeping jet actuator.

* Corresponding Author

compared to the existing vertical tails in operation. The controllability of the rudder was studied recently in the typical twin-engine aircraft. The results of this test shown that the SWJ actuator placed in the vertical tail can increase the controllability up to 18% and the mass flow required to apply in the inlet is reasonable. Recently, the time-resolved internal and external flow of the fluidic oscillator has been analyzed using PIV data [15]. The result of this study provides a good guideline for the development and optimization of future oscillator's devices, and show that the inner geometry is crucial to optimize the SWJ [16].

In spring 2015, the first flight test of the Boeing 757 ecoDemostrator [17] of the NASA ERA17 project was performed. The 757 ecoDemostrator included 31 sweeping jet actuators on the starboard side of the vertical tail. The main purpose of the flight test was to demonstrate the effectiveness and the integration of the active flow control into the airframe. Pilot feedbacks and engineering analysis confirmed that the active flow control is effective and it enhanced the rudder controllability with force increase up to 16% for high rudder deflection angle. The results of ecoDemostrator test verify the application of the active flow control for the vertical tail; however, the complex flow inside the SWJ has to be understood for designing optimized actuator geometry with minimum pressure loss. In this study, numerical studies using computational fluid dynamics method are performed to investigate the effects of the mass flow rate and the inner geometry.

The Coanda effect [18, 19] is one crucial fluidic principle that occurs in this type of oscillators. The jet flow attaches to the inner surfaces in an alternating manner as illustrated in Figure 1. In the SWJ actuator core region, the jet flow switches between the curved surfaces. The surface geometry is a critical parameter on SWJ actuator design since it will determine jet flow direction in the core regions. A parametric study of the internal surface geometry (Coanda Surface) of the SWJ actuator performed in this paper. The pressure increases in the feedback channel and pushes the main jet entering the core area to the other Coanda surface. The vortex created by the sharp corner also helps the switching. This process happens cyclically. Design of the inner Coanda surfaces is critical for the oscillation process, but there is no design and optimization study available in the literature [20]. The fluid oscillation of the flow is an essential physical process because it determines the extent of the attachment region of the Coanda effect. The walls interacting with the flow are important in the turbulent flows because they contain a boundary-layer near the wall which interacts with the free shear layers. These layers are growing less than the free jet width, and this determines the velocity fluctuation damping from the outer layer and generates the jet oscillations inside the device as shown in Figure 1. The optimization of the Coanda surface will help to give the best output flow of sweeping jet and also will help to understand the fluidic vectoring of the SWJ which developed in this study.

2. METHODOLOGY

The governing equations for conservation of mass, momentum, and energy assuming fully turbulent, compressible flow are solved using computational fluid dynamics software, Ansys Fluent v17. A two-dimensional SWJ actuator geometry and computational domain are created using the Design Modeler software as shown in Figure 2. The SWJ actuator geometry is provided by Kara [5] and has an exit nozzle throat height of 6.35 mm. A semi-circular domain with a radius of 600 mm is placed at the downstream of the SWJ actuator geometry. In Figure 2, parameters D1 and D2 represent feedback channel height and width, which are 7.42 mm and 6.83 mm respectively, and remain constant for all simulations. The parameters D1 and D2 were varied systematically to investigate the effect of feedback channel geometry on jet oscillation frequency by Jurewicz [9]. The origin is located in the cross-section of the SWJ actuator symmetry line and exit plane as shown in Figure 2. To perform a detailed analysis, data sampling points are placed at the downstream of exit nozzle, namely, at (3 mm, 0), (6 mm, 0), (6 mm, 10 mm), and (6 mm, -10 mm) as shown in Figure 2-b. Three lines are set up to measure the mass flow rate in the feedback channels and at the exit nozzle throat. At these locations, the total and static pressures variations over time are sampled at the midpoints.

Computational meshes are created by Ansys Meshing software in a semi-automatic way for different inner geometric surfaces. The mesh has a two level of element refinement using a sphere of influence method as shown in Figure 3. The inner refinement (body sizing 2) covering SWJ actuator geometry has a radius of 37 mm with an element size of 0.2 mm, and outer refinement (body sizing 1) has a radius of 130 mm with an element size of 1 mm. The boundary-layer mesh is created on the solid walls using 20 layers with a growth rate of 1.15. The first layer height is set as $5x10^{-3}$ mm. The average value of y+ is found ranging between 0.2 and 5. Boundary conditions for all of the solid surfaces are defined as no-slip, no-penetration for velocity, and adiabatic for temperature. Figure 2 and Figure 3 shows mass flow inlet (implemented as mass flux due to two-dimensional geometry), pressure outlet and wall boundaries in addition to sampling points and lines for velocity profile plots, and Table 1 summarizes the numerical values of boundary conditions. The pressure outlet is assumed to open to the ambient environment at P_∞=101,325 Pa, and T_∞=298.16 K. A pressure gradient of 5 Pa is applied between outlet boundaries to create a surrounding flow in the streamwise direction (+x) in order to help the flow to develop in this direction and help to the simulation to converge faster.

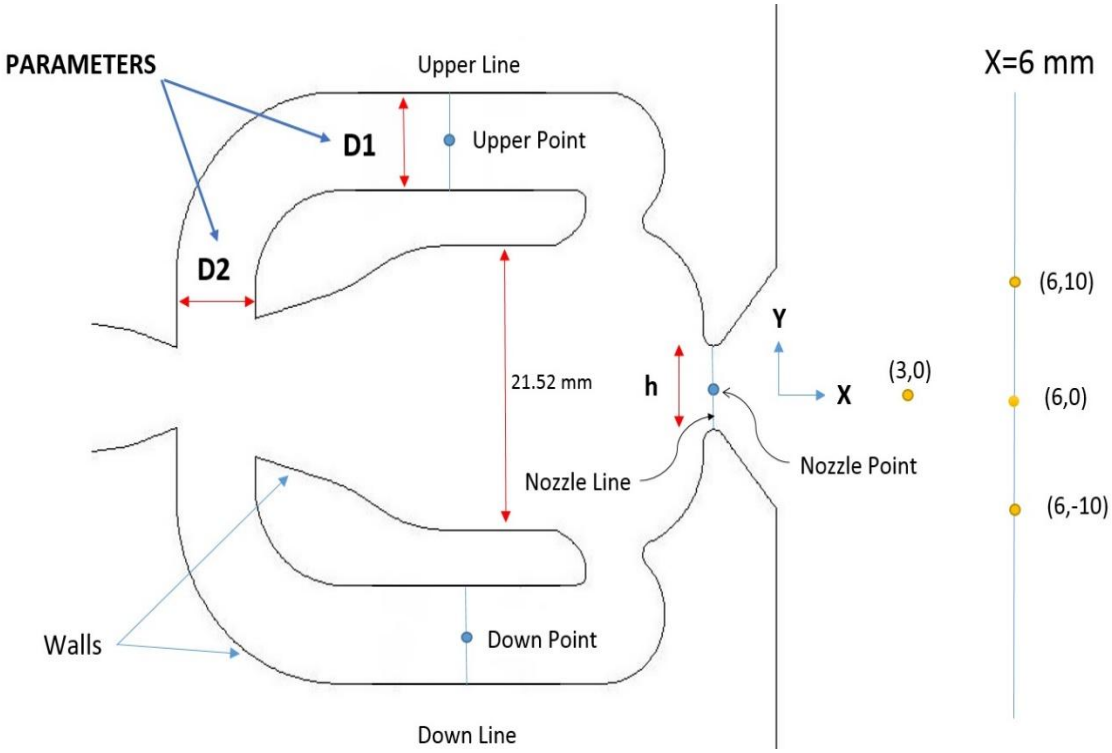

Figure 2. Computational set up.

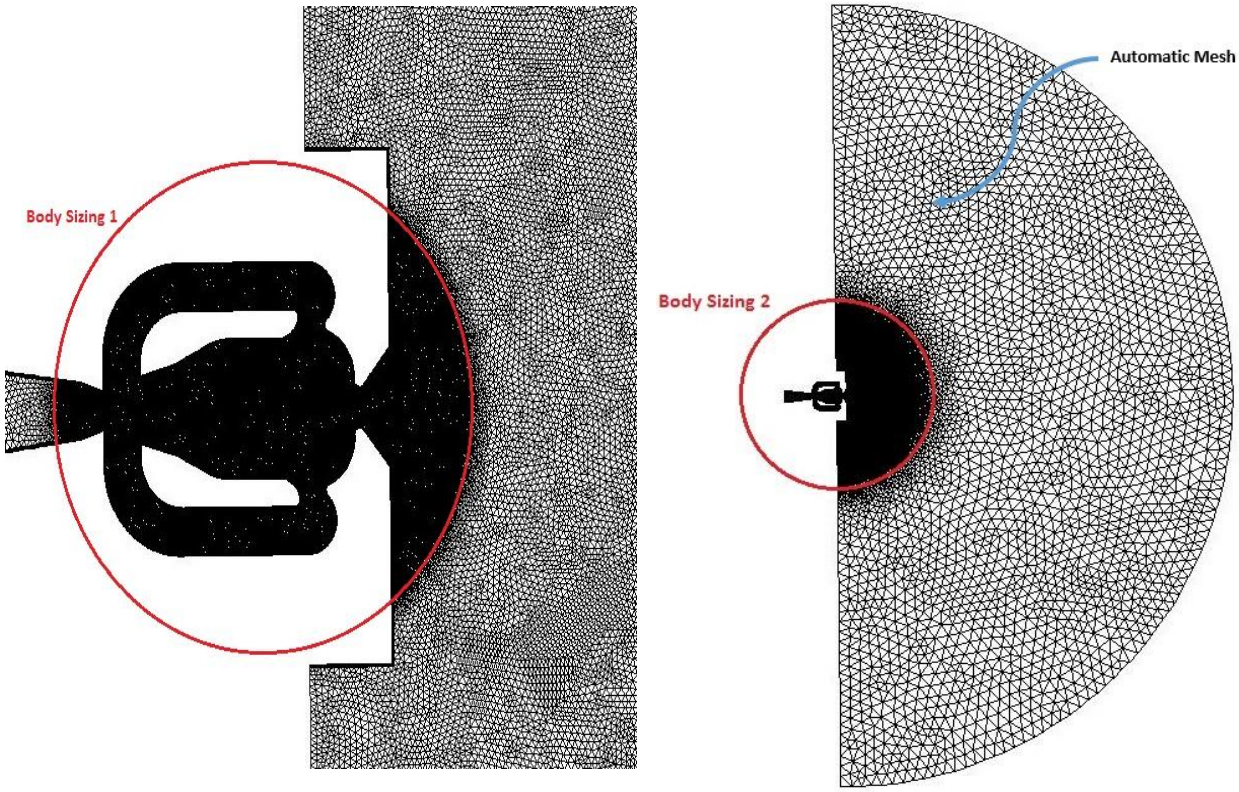

Figure 3. Mesh used for computations and close up view of the SWJ actuator.

Table 1. Boundary conditions.

P	Pa	101327.5			Outlet static pressure, downstream
T	ºK	298.16			Outlet static temperature
h	mm	6.35			Exit nozzle throat height
d	mm	6.35			Depth
h_i	mm	16.21			Inlet channel height
A_i	mm^2	102.934			Inlet cross section area
$\dot{m}$	lb/s	0.010	0.015	0.020	Mass flow rate
mass flux	kg/(m^2 s)	44.067	66.100	88.133	Mass flux
V_i	m/s	37.2	55.8	74.4	Inlet velocity
M_i		0.108	0.161	0.215	Inlet Mach number

The Coanda Surface represented in Figure 4 is the main surface studied in this paper. The surfaces change for different geometries as represented in Figure 5 a-h. The original SWJ actuator geometry is provided by Kara [20] and is represented in Figure 4.

All the simulations are performed for a fully-turbulent, compressible flow using the computational fluid dynamics software Fluent v17. Pressure based, coupled, time-dependent solver with a constant time step of $\Delta t=10^{-5}$ seconds is employed. Time accurate simulations are performed using the bounded second-order implicit scheme. The second-order discretization for pressure and the second-order-upwind formulation for density, momentum, turbulent kinetic energy, specific dissipation rate, and energy are adopted. The Shear Stress Transport (SST) k-ω turbulence model is applied. Simulations initialized using the inlet conditions and run for 5,000 time-steps to get oscillating flow. Then simulations continued for another 10,000-time step (0.1 s), to generate a database from which statistically converged flow quantities could be analyzed.

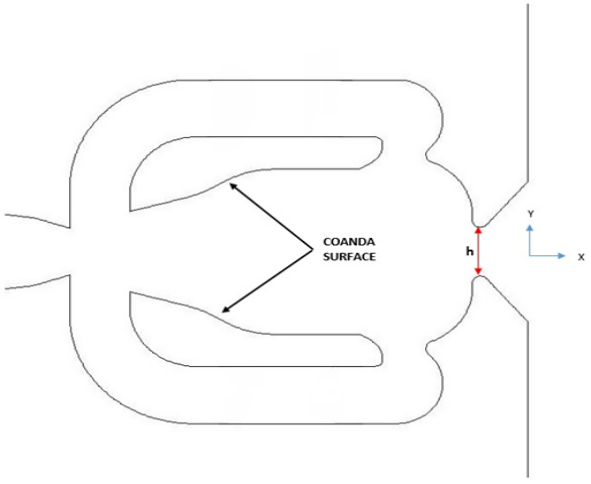

Figure 4. Original geometry SWJ (Case 1, Baseline).

3. RESULTS

3.1 Pressure Inlet Study

Employing the numerical model described in the previous section, simulations are run for a mass flow rate of 0.015 lb/s for the baseline and modified SWJ actuator geometries shown in Figure 5. The static mean pressure at the inlet, at the downstream of exit nozzle and the differences are presented in Table 2 for different Coanda surfaces. The Figures 6a-h and 7a-h show the mean static and mean total pressure contours of the cases analyzed. The results indicate that Case 7 has the minimum mean static pressure drop while Case 2 has the maximum. Comparison of the mean static and mean total pressure drop along the symmetry line (y=0) is shown in Figures 8 and 9. It is evident that the geometry of the Coanda surfaces can modify the mean static pressure drop by 14% at the prescribed mass flow rate of 0.015 lb/s.

Similarly, the mean total pressure drop between the mass flow inlet boundary and the origin located downstream of the SWJ actuator exit nozzle are analyzed and results are presented in Table 3. Instantaneous total pressure contours for baseline and modified geometries are shown in Figure 7 which shows the pressure drop mechanisms in a more clear way compared to static pressure contours. In Figure 7-a, the jet enters the SWJ actuator core area and move towards the upper Coanda surface. Further downstream, the jet braches out to two parts. While the smaller jet provides flow for the feedback channel, remaining jet left the exit nozzle at an angle. The time of the instantaneous snapshots are not synchronized for various cases to enable the reader to observe different phases of the internal flow structures and jet branching-outs.

There are two important cases highlighted in Table 3. The Case 7 shows the minimum mean total pressure drop (20934.7 Pa, and 19.9% less than the baseline).

On the other hand, the Case 2 shows the maximum mean total pressure difference with the value of 27248.8 Pa and 4.26% greater than the baseline. Therefore, the Case 7 provides an efficient alternative to the original SWJ actuator geometry.

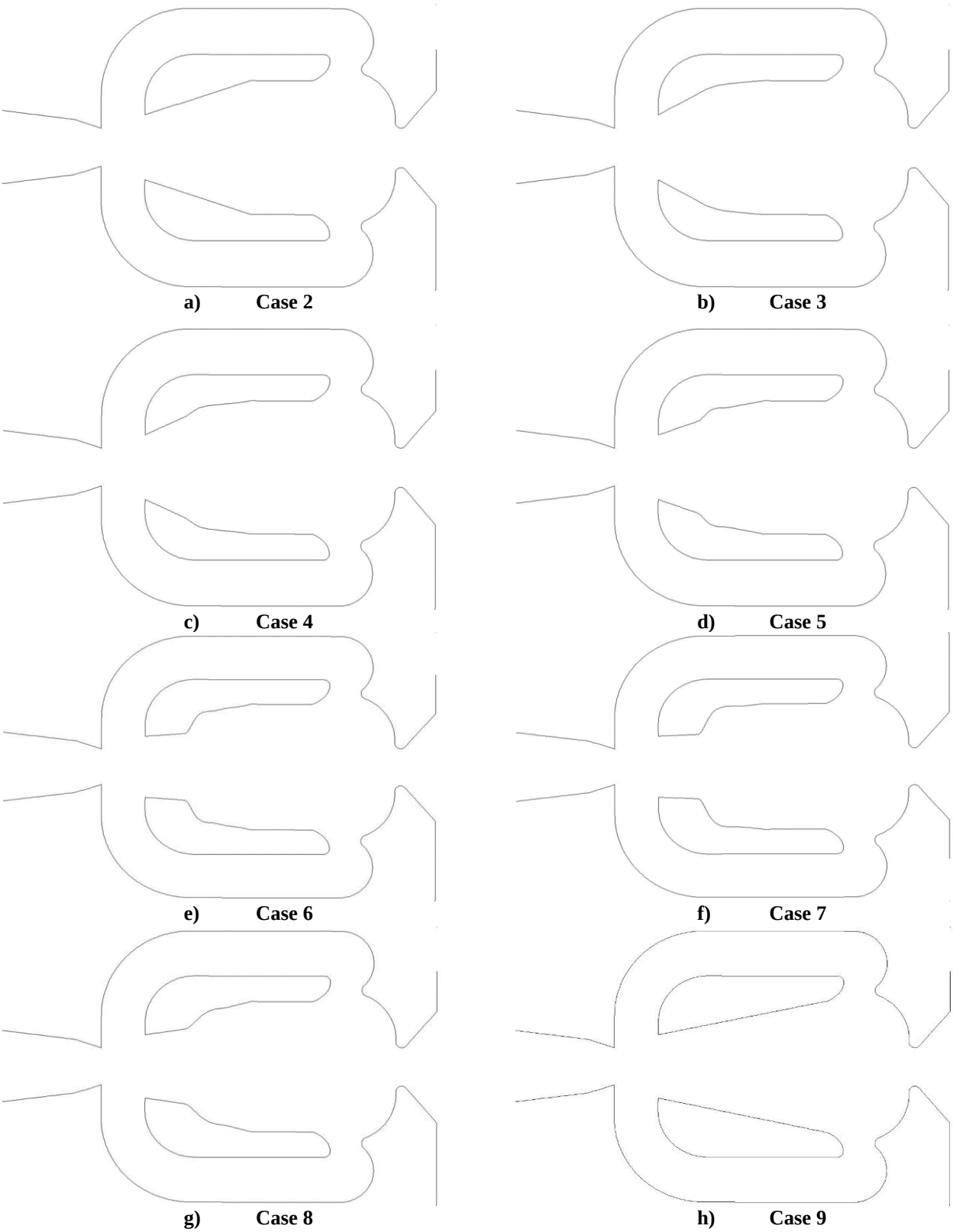

Figure 5. Different Coanda surfaces in the SWJ.

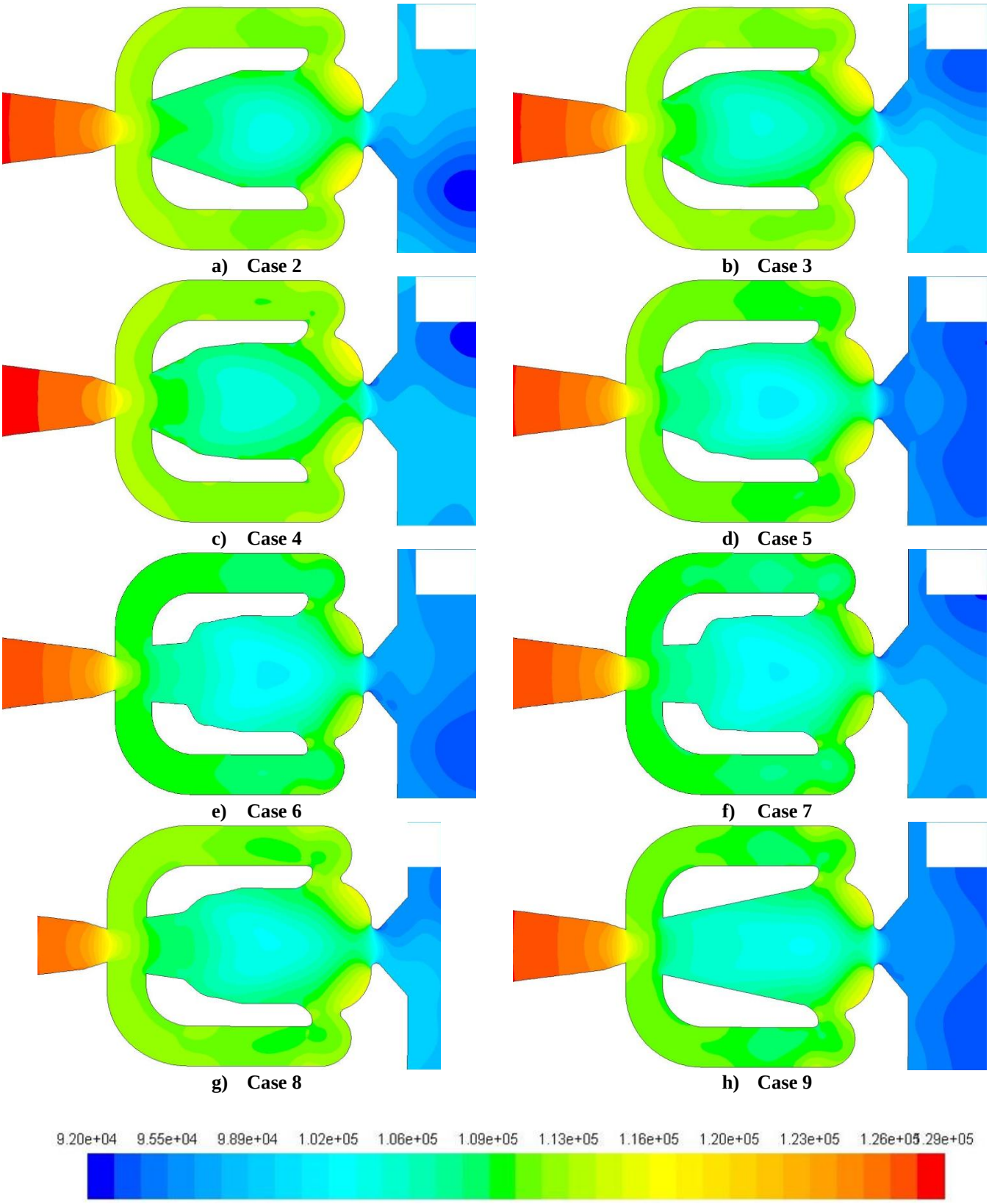

Figure 6. Time averaged static pressure contours for different Coanda surfaces.

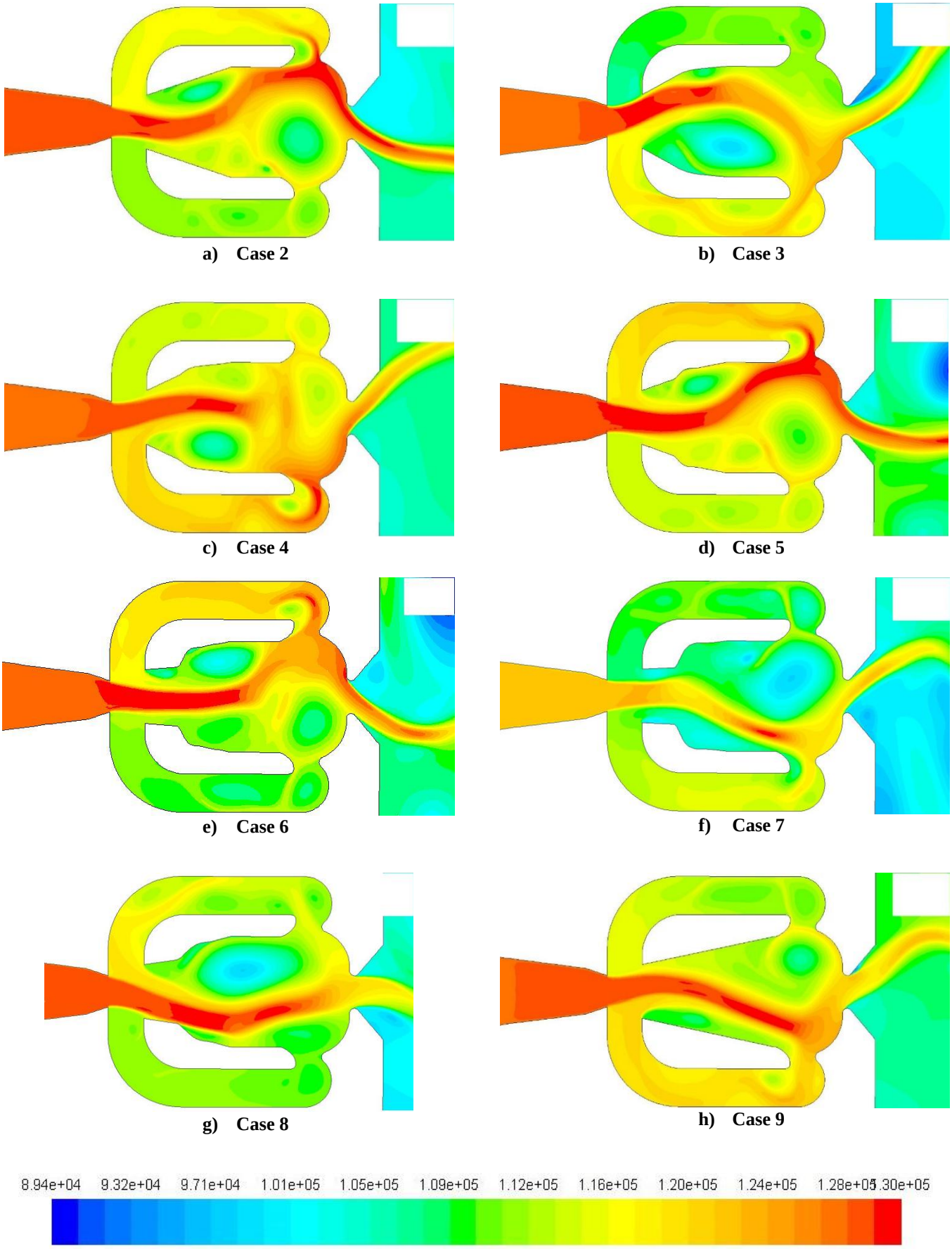

Figure 7. Instantaneous total pressure contours for different Coanda Surfaces.

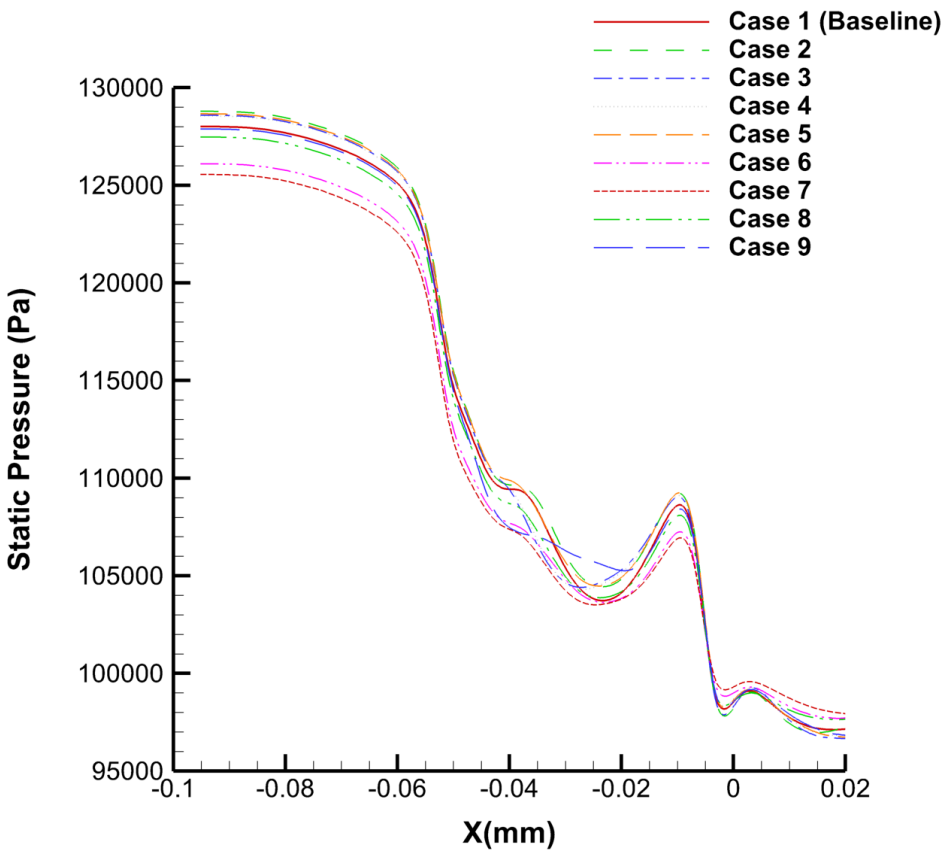

Figure 8. Variation of the mean static pressure along the x-axis for different SWJ actuators.

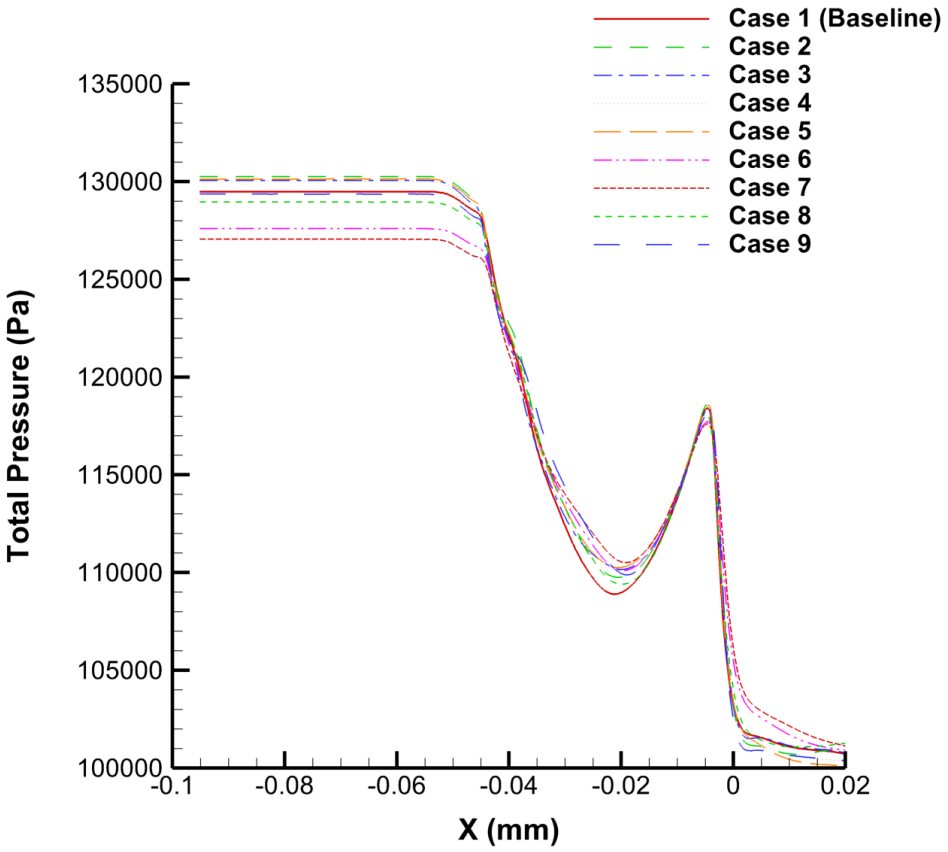

Figure 9. Comparison of mean total pressure drop for SWJ actuators.

3.2 Effect of Coanda Surface Geometry on Jet Oscillation Frequency

In this section, the effect of the Coanda surface on the outflow jet frequency is studied. The Coanda surfaces from Figure 4 are identified as key parameters for initial studies and further optimization. Since the SWJ actuator geometry is symmetric about the x-axis, the top and bottom channels, and the inner surfaces are designed to have the same dimensions. Nine new geometry with different Coanda surfaces are created, meshed, and simulated using a mass flow rate of 0.015 lb/s. Time histories of velocity magnitude at the points (6mm, 0mm), (6mm, 10mm) and (6mm, -10mm) are recorded. Figure 11 shows the time history of velocity magnitude for Case 1 (baseline) at the point (6mm, 0mm).

Time history of velocity magnitude shows periodic fluctuations. The Fast Fourier Transform (FFT) analysis is done to find the jet oscillation frequency for all the cases. In order to realize an appropriate FFT analysis, the signal is clipped for reducing the noise. The first harmonic is determined by the largest peak in the amplitude is 346.32 Hz as shown in Figure 12. Higher harmonics are also visible in the spectrum. Table 4 shows the effect of the Coanda surface geometry on the jet oscillation frequency for a mass flow rate of 0.015 lb/s. The first harmonic varies with the Coanda surface for all cases. The Case 9 has the highest frequency and Case 7 has the lowest frequency as shown in Figure 13. Case 7 has the lowest pressure loss as discussed in the previous section. Case 2 has the same frequency with the baseline but has higher total pressure loss as shown in Table 2. These results show that the Coanda Surface affect the frequency of the jet oscillation as well.

Figure 10 represents the comparison of different frequencies available in the data literature [9, 16, 20, 21]. The analysis made in this section is matching closely with experimental results. All the computational techniques employed in the literature shown higher frequency that the experimental results available. The computational frequency predictions lay between $\pm 15\%$ of the experimental results.

3.3 Study for Different Mass Flow Rates

The frequency response of oscillating jet from a sweeping jet actuator mainly depends on the actuator geometry and mass flow rate. In order to understand the relationship between frequency, mass flow rate and internal geometric parameters, flow simulations with three different mass flow rate for varying inner Coanda Surface are performed. In this section, the computational mesh is created using the parameters as explained in the previous section. Details of fully-turbulent 2D Unsteady RANS simulations are explained in previous sections. The simulations are run for mass flow rates of 0.010 lb/s, 0.015 lb/s, and 0.020 lb/s. Each simulation is performed, first, for 5,000 steps without data sampling and after 10,000 steps with data sampling. The values of the frequencies for different mass flow rates are presented in Table 5. The effect of the inner Coanda Surface geometry of each

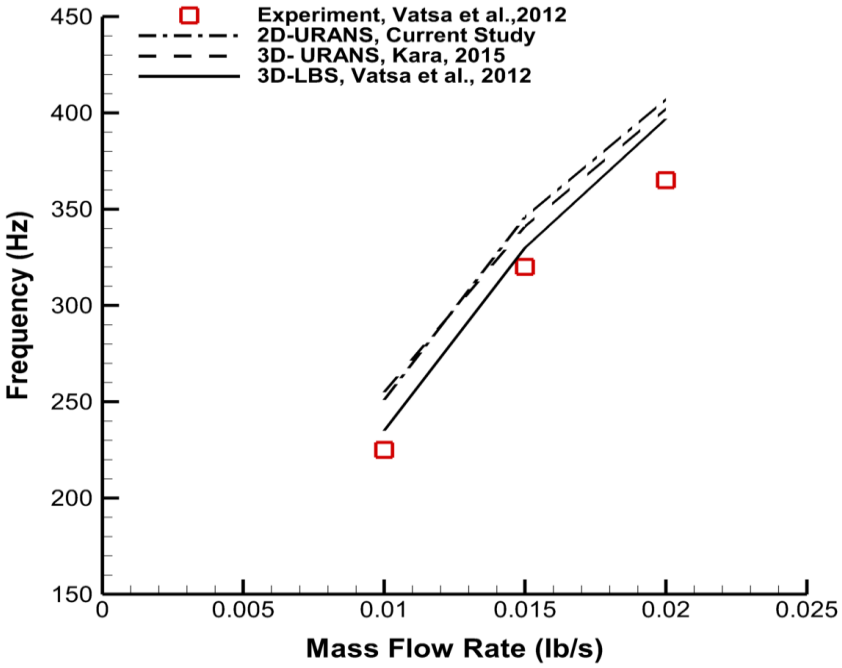

Figure 10. Comparison of jet oscillation frequency with available data in the literature for baseline geometry.

case is shown in Figure 14 and is appreciated the linearity of the oscillating frequency versus the mass flow rate. For higher mass flow rate the linearity is becoming perturbed.

4. CONCLUSIONS

In this study, unsteady flow fields generated by Sweeping Jet (SWJ) actuator are investigated using two-dimensional, unsteady, Reynolds-Averaged Navier Stokes (2D-URANS) simulations with Ansys v17.0 Fluent Software. The Sweeping Jet Actuator geometry is represented using 211 thousand Quad4 and Tri3 elements. Hybrid grid enables to describe complete geometric details of complex SWJ actuator geometry. Using 2D-URANS simulations, unsteady internal and external flows of SWJ actuator are analyzed with different inner Coanda Surfaces. The effect of different Coanda Surfaces, as well as inlet mass flow rates, on the jet velocity magnitude and in the oscillating frequency, were presented. The oscillating jet frequencies of the SWJ actuator are obtained from the time history of velocity magnitude using FFT analysis for all three mass flow rate conditions (0.010 lb/s, 0.015 lb/s, and 0.020 lb/s) with various inner Coanda Surfaces. The mean static pressure and mean total pressure variations are calculated to obtain the pressure losses between the inlet and the outlet with different SWJ actuators. The results in Section 3 show that the Case 7 can save around 19.89% of the total pressure respect the baseline geometry as shown in Table 3.

Table 2. Mean static pressure**.**

	Mean Static Pressure Inlet (Pa)	Mean Static Pressure in the point (0,0) (Pa)	Difference (Pa)
Case 1	128017	98502.1	29514.9
Case 2	**128795**	**98222.3**	**30572.7**
Case 3	128594	98369.6	30224.4
Case 4	128558	98691.1	29866.9
Case 5	128666	98636.3	30029.7
Case 6	126108	98998.5	27109.5
Case 7	**125561**	**99306.2**	**26254.8**
Case 8	127479	98567.7	28911.3
Case 9	127890	98561.9	29328.1

Table 3. Mean total pressure drop.

	Mean Total Pressure Inlet (Pa)	Mean Total Pressure on the point (0,0) (Pa)	Difference (Pa)	Difference %
Case 1	129492.7	103358.8	26133.9	---
Case 2	**130261.9**	**103013.1**	**27248.8**	**+4.3**
Case 3	130063.4	102960.9	27102.5	+3.7
Case 4	130027.6	103467.8	26559.8	+1.6
Case 5	130133.8	103404.0	26729.8	+2.3
Case 6	127606.7	105387.6	22219.1	-15.0
Case 7	**127066.4**	**106131.7**	**20934.7**	**-19.9**
Case 8	128961.2	104030.4	24930.8	-4.6
Case 9	129367.0	102480.6	26886.4	+2.9

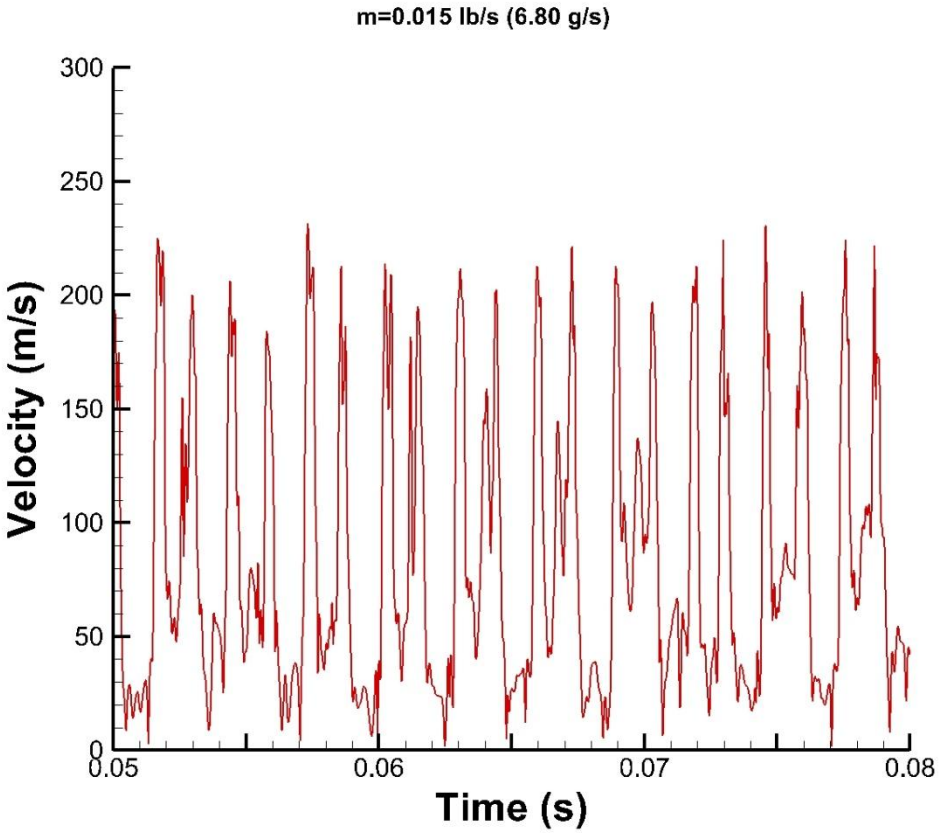

Figure 11. Time history of velocity magnitude at the sampling point (6mm, 0) for Case 1.

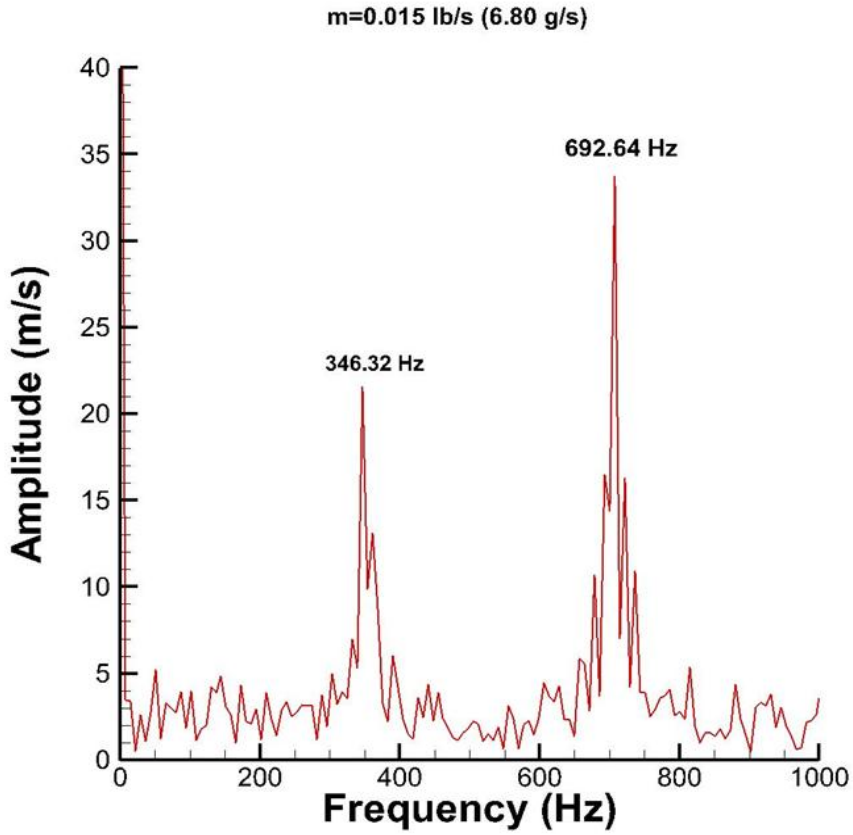

Figure 12. FFT analysis of velocity magnitude sampled at point (6mm, 0) for Case 1.

Table 4. Jet oscillation frequency
(mass flow rate of 0.0015 lb/s).

	Jet Oscillation Frequency (Hz)
Case 1	346.32
Case 2	346.32
Case 3	339.10
Case 4	346.32
Case 5	352.56
Case 6	341.88
Case 7	**328.28**
Case 8	346.32
Case 9	**352.56**

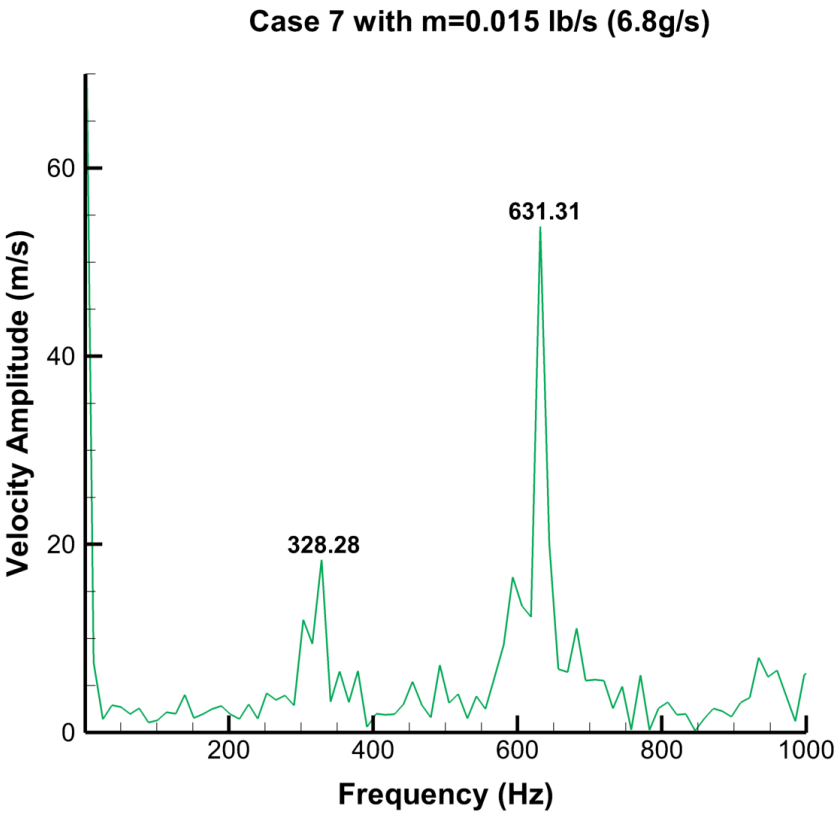

Figure 13. FFT analysis of velocity magnitude sampled at point (6mm, 0) for Case 7.

Table 5. Comparison of jet oscillation frequency for the mass flow rate values of 0.010 lb/s, 0.015 lb/s and 0.020 lb/s.

	Mass Flow Rate		
lb/s *(g/s)*	***0.010*** *(4.54)*	***0.015*** *(6.80)*	***0.020*** *(9.07)*
Case 1 (Baseline)	251.83	346.32	407.59
Case 2	**252.52**	**346.32**	**418.47**
Case 3	252.81	339.1	382.39
Case 4	256.41	346.32	447.33
Case 5	266.95	352.56	454.54
Case 6	245.31	341.88	375.18
Case 7	**227.27**	**328.28**	**418.47**
Case 8	245.72	346.32	391.41
Case 9	259.74	352.56	425.68

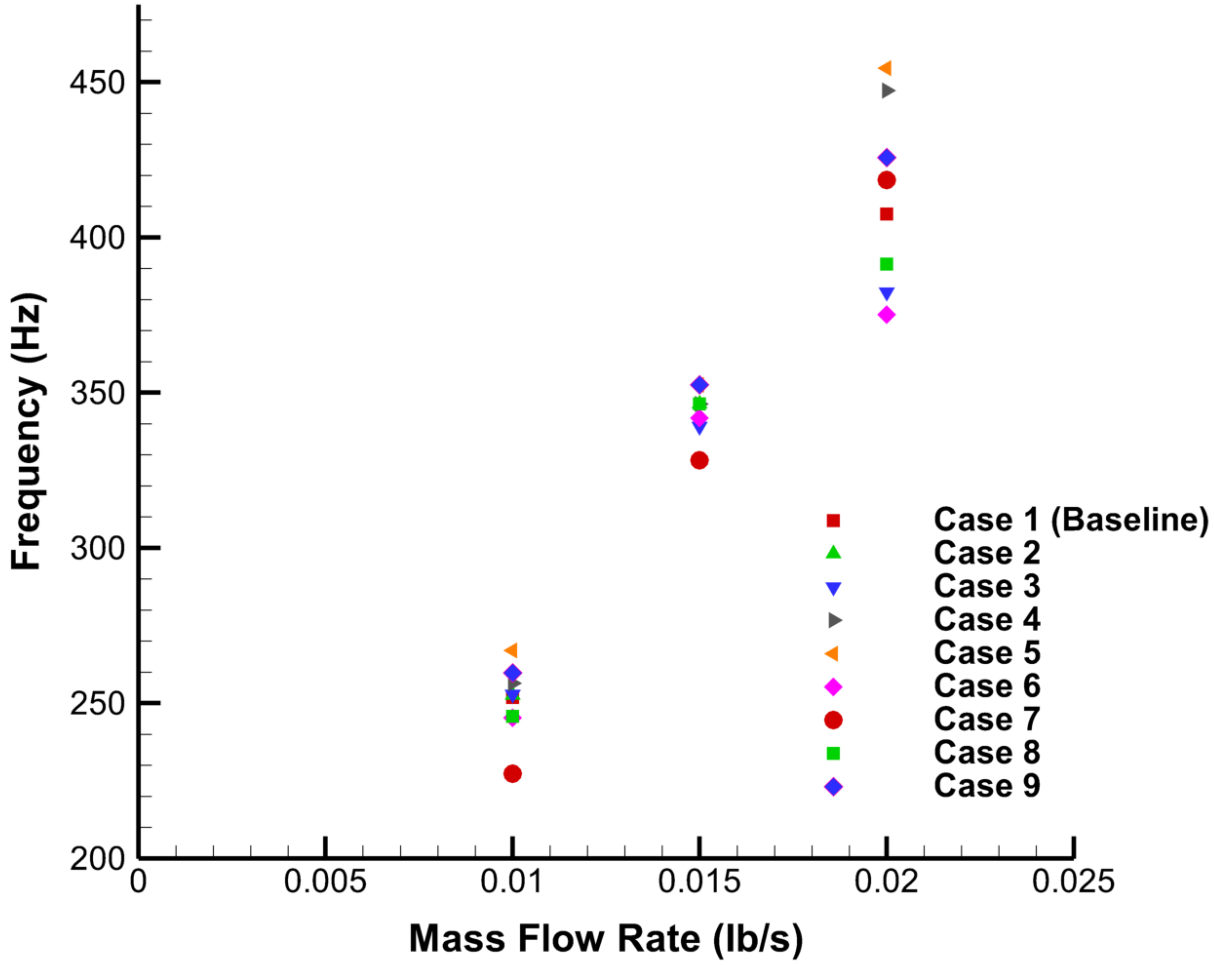

Figure 14. Comparison of jet oscillation frequency at different mass flow rates.

ACKNOWLEDGEMENTS

The authors would like to thank KURIF program of the Khalifa University of Science Technology and Research for funding the research work.

6. REFERENCES

[1] Monechi, B., Servedio, V. D. P., and Loreto, V., "Congestion transition in air traffic networks," *PLoS ONE*, vol. 10, 2015.

[2] Abbas, A., De Vicente, J., and Valero, E., "Aerodynamic technologies to improve aircraft performance," *Aerospace Science and Technology*, vol. 28, 2013, pp. 100–132.

[3] Cattafesta, L. N., and Sheplak, M., "Actuators for Active Flow Control," *Annual Review of Fluid Mechanics*, vol. 43, 2011, pp. 247–272.

[4] Graff, E., Seele, R., Lin, J., and Wygnanski, I., "Sweeping Jet Actuators - a New Design Tool for High Lift Generation," *Innovative Control Effectors for Military Vehicles (AVT-215)*, 2013, pp. 1–25.

[5] Kara, K., "Flow separation control using sweeping jet actuator," *35th AIAA Applied Aerodynamics Conference, 2017*, 2017.

[6] Slupski, B. J., and Kara, K., "Separated flow control over Naca 0015 airfoil using sweeping jet actuator," *35th AIAA Applied Aerodynamics Conference, 2017*, 2017.

[7] Bobusch, B., Woszidlo, R., Bergada, J., Nayeri, C., and Paschereit, C., "Experimental study of the internal flow structures inside a fluidic oscillator," *Experiments in Fluids*, vol. 54, 2013, pp. 1559–1571.

[8] Slupski, B. J., and Kara, K., "Design of a Sweeping Jet Actuator for Improved Aerodynamic Performance," *The 3rd International Aviation Management Conference 2016*, Dubai, United Arab Emirates: Emirates Aviation University, 2016, p. 156.

[9] Slupski, B. Z., and Kara, K., "Effects of Geometric Parameters on Performance of Sweeping Jet Actuator," *34th AIAA Applied Aerodynamics Conference*, American Institute of Aeronautics and Astronautics, 2016.

[10] Tesař, V., and Smyk, E., "Fluidic low-frequency oscillator with vortex spin-up time delay," *Chemical Engineering and Processing: Process Intensification*, vol. 90, 2015, pp. 6–15.

[11] Lin, J. C., Andino, M. Y., Alexander, M. G., Whalen, E. A., Spoor, M. A., Tran, J. T., and Wygnanski, I. J., "An Overview of Active Flow Control Enhanced Vertical Tail Technology Development," *54th AIAA Aerospace Sciences Meeting*, 2016, pp. 1–13.

[12] Arnold, T., Cafarelli, D., Gurung, S., Kwong, A., and Nippard, J., "Performance Enhancement of a Full-scale Vertical Tail with Active Flow Control TeModelchnology," *53rd AIAA Aerospace Sciences Meeting*, 2015, pp. 1–11.

[13] Andino, M., Lin, J., Washburn, A., Whalen, E., Graff, E., and Wygnanski, I., "Flow Separation Control on a Full-Scale Vertical Tail Model using Sweeping Jet Actuators," *53rd AIAA Aerospace Sciences Meeting*, 2015, pp. 1–14.

[14] Rathay, N. W., Boucher, M. J., Amitay, M., and Whalen, E., "Performance Enhancement of a Vertical Tail Using Synthetic Jet Actuators," *AIAA Journal*, vol. 52, 2014, pp. 810–820.

[15] Woszidlo, R., Ostermann, F., Nayeri, C. N., and Paschereit, C. O., "The time-resolved natural flow field of a fluidic oscillator," *Experiments in Fluids*, vol. 56, 2015, p. 125.

[16] Slupski, B. J., and Kara, K., "Effects of Feedback Channels and Coanda Surfaces on the Performance of Sweeping Jet Actuator," *55th AIAA Aerospace Sciences Meeting*, 2017.

[17] A. Whalen, E., Spoor, M., M. Vijgen, P., Tran, J., Shmilovich, A., C. Lin, J., and Andino, M., "Full-scale Flight Demonstration of an Active Flow Control Enhanced Vertical Tail," 2016.

[18] Katz, P., "The Coanda effect," *Gesundheits-Ingenieur*, vol. 94, 1973, pp. 169–174.

[19] Palmer, M., "The Coanda effect," *International Water Power and Dam Construction*, vol. 56, 2004, pp. 10–13.

[20] Kara, K., "Numerical Study of Internal Flow Structures in a Sweeping Jet Actuator," *33rd AIAA Applied Aerodynamics Conference AIAA*, 2015, pp. 1–17.

[21] Vatsa, V., Koklu, M., and Wygnanski, I., "Numerical Simulation of Fluidic Actuators for Flow Control Applications," *6th AIAA Flow Control Conference*, 2012.

VITAE

Mr. Bartosz JUREWICZ SLUPSKI, PhD Candidate.

Mr. Bartosz Jurewicz Slupski is currently completing his Ph.D. at the Khalifa University in Abu Dhabi, UAE under the supervision of Dr. Kursat Kara. Mr.

Bartosz graduated in BEng and MEng in Aeronautical Engineering from Technical University of Madrid (UPM). During his MEng he spent one year at Tongji University in Shanghai (China) like exchange student where he has done his MEng Thesis : "The Landing Gear: Design, Features and Electric Green Taxiing System" in collaboration and supervision of Dr. Xu Zhenyu, associate professor of School of Aerospace Engineering and Applied Mechanics (SAEAM) of this University. During his studies, Mr. Bartosz worked in Repsol S.A Company as an intern in the department of renewal energy and collaborate in the innovative bladeless turbine project called 'Vortex' turbine. Also, Mr. Bartosz spends summer internship in Manipal Institute of Technology in Manipal (India) as a research assistant in the aerospace department. The research interest fields of Mr. Bartosz are applied aerodynamics, Flow Control, Computational Fluid Dynamics and Aeronautical Propulsion.

Dr. Kursat KARA, Ph.D.

Kursat KARA is an Assistant Professor of Aerospace Engineering at the Khalifa University, Abu Dhabi, UAE. He received his BS and MS degrees from Istanbul Technical University and a Ph.D. degree from Old Dominion University, Norfolk, VA, USA in 2008. His doctoral dissertation was on hypersonic boundary layer receptivity to acoustic disturbances over cones. Following graduation, he was a research engineer at New England Analytics LLC, Shelton, CT consulting company to Sikorsky Aircraft Corp. He then joined the Aerospace Engineering Department at Penn State as a post-doctoral research associate and worked with Prof. Philip J. Morris. In 2010, he joined Khalifa University. Dr. Kara's research interests include computational aerodynamics / fluid dynamics, hypersonic boundary-layer transition (DNS), supersonic hot jet simulations for aeroacoustics (DES), high order accurate schemes (WENO, DRP), active flow control wind turbine blades (with Dr. Sankar from Georgia Tech), wind energy and spray cooling of electronics. His research has been funded by the NASA Langley Research Center, the U.S. Navy Naval Air Systems Command (NAVAIR) and Khalifa University. Dr. Kara is a Senior Member of AIAA, Member of AIAA Applied Aerodynamics Technical Committee, and the technical chair of 34th Applied Aerodynamics Conference (June 2016, Washington DC, USA).